DOI: 10.1002/chem.200500288

Highly Stable Neutral and Positively Charged Dicarbollide Sandwich Complexes

Rosario Núñez,[a] Oscar Tutusaus,[a] Francesc Teixidor,*[a] Clara Viñas,[a] Reijo Sillanpää,[b] and Raikko Kivekäs[c]

Abstract: Novel sandwich metallacarboranes *commo*-[3,3′-Ni(8-SMe_2-1,2-$C_2B_9H_{10})_2$] (**1**), *commo*-[3,3′-Co(8-SMe_2-1,2-$C_2B_9H_{10})_2]^+$ (**2**$^+$), *commo*-[3,3′-Ru(8-SMe_2-1,2-$C_2B_9H_{10})_2$] (**4**) and *commo*-[3,3′-Fe(8-SMe_2-1,2-$C_2B_9H_{10})_2$] (**5**) have been prepared by reaction of [10-SMe_2-7,8-*nido*-$C_2B_9H_{10}]^-$ with $NiCl_2{\cdot}6H_2O$, $CoCl_2$, [$RuCl_2$(dmso)$_4$] and [$FeCl_2$(dppe)], respectively. Reduction of **2**$^+$ with metallic Zn leads to the neutral and isolable complex *commo*-[3,3′-Co(8-SMe_2-1,2-$C_2B_9H_{10})_2$] (**3**). Theoretical calculations using the ZINDO/1 semiempirical method show three energy minima for complexes **1**–**3** and **5** that agree with the presence of three different rotamers in solution at low temperature, while four relative energy minima have been found for **4**. The calculated rotational energy barriers for complexes **1**–**5** have been found in the range 5.2 ± 0.2 and 11.5 ± 0.2 kcal mol^{-1}. These values are in agreement with the experimental data calculated for complexes **2**$^+$ and **5**. Only one rotamer is found in the X-ray crystal structure of complexes **1**–**3**, while two are observed for **4**. Neutral complexes **1**, **3** and **4** exhibit a *gauche* conformation, whereas a *cisoid* conformation is found for the **2**$^+$ ion. Rotamers evident from X-ray diffraction studies are in agreement with the global energy minimum calculated by the ZINDO/1 method. The electrochemical studies conducted on **1**, **3**, **4** and **5** support the proposal that the charge-compensated ligand [10-SMe_2-7,8-*nido*-$C_2B_9H_{10}]^-$ stabilises lower oxidation states in metals than the dianionic [7,8-*nido*-$C_2B_9H_{11}]^{2-}$ and even the $[C_5H_5]^-$ ligands.

Keywords: boron · carboranes · conformation analysis · electrochemistry · sandwich complexes

Introduction

Boron cluster ligands provide structural and bonding possibilities distinct from conventional organic ligands.[1] The best known of the boron ligands is the dicarbollide dianion [7,8-*nido*-$C_2B_9H_{11}]^{2-}$ (Dcb^{2-}), although there are other known smaller icosahedral ligands, such as the *nido*-$[C_2B_4H_6]^{2-}$. Much has been written about the analogy between the dicarbollide [7,8-*nido*-$C_2B_9H_{11}]^{2-}$ and the isoelectronic cyclopentadienide ions $[C_5H_5]^-$ (Cp^-) and their metal complexes.[1e,2] The Dcb^{2-} ligand is formally equivalent to the Cp^- ligand and both are able to coordinate in a η^5-bonding fashion. The synthesis and properties of the first Dcb^{2-} sandwich complexes, analogous to metallocenes, were reported in 1965, and for *nido*-$[C_2B_4H_6]^{2-}$ in 1976.[3] Dcb^{2-} sandwich complexes with first-row transition-metals such as Fe^{II},[4] Co^{III},[4,5] Ni^{III},[4,6] Ni^{IV},[4,6d,7] Cu^{II},[8] Cu^{III},[8] Cr^{III}[9] and Co^{II}[10] have been synthesised and fully characterised. In addition, some *nido*-$[C_2B_4H_6]^{2-}$ sandwich metallacarboranes of iron, cobalt and nickel have been also reported.[11] Molecular orbital (MO) calculations confirmed the analogy of metallocenes and the metal–dicarbollide analogues.[12] However, comparative redox properties of metallocenes and metal–Dcb^{2-} sandwich compounds have shown that the latter are oxidised more easily.[13] This is why it is considered that the Dcb^{2-} ligand stabilises high formal oxidation states.[14] This stabilisation may be related to the higher charge in Dcb^{2-} than that of Cp^-. The charge difference may be surpassed by introducing a charge-compensating group in Dcb^{2-}. Although charge-compensated [*x*-L-7,8-*nido*-$C_2B_9H_{10}]^-$ ($x=7$,

[a] Dr. R. Núñez, Dr. O. Tutusaus, Prof. F. Teixidor, Dr. C. Viñas
Institut de Ciència de Materials de Barcelona
Consejo Superior de Investigaciones Científicas
Campus de U.A.B., Bellaterra, 08193 Barcelona (Spain)
Fax: (+34) 93-580-57-29
E-mail: teixidor@icmab.es

[b] Prof. R. Sillanpää
Department of Chemistry
University of Jyväskylä
40351 Jyväskylä (Finland)

[c] Dr. R. Kivekäs
Inorganic Chemistry Laboratory
Box 55, University of Helsinki
00014 Helsinki (Finland)

9, 10; L = pyridine, THF, SR_2, PPh_3 and so on) monoanionic ligands have been studied,[15] few transition-metal sandwich complexes have been reported.[15d,16,17] To compare the properties of monoanionic derivatives of Dcb^{2-} with metallocene analogues, we have recently reported the preparation of half-sandwich ruthenacarborane complexes with [10-SR_2-7,8-*nido*-$C_2B_9H_{10}]^-$ (R = Me, Et, $(CH_2)_4$, EtPh) similar to $[RuCl(Cp)(PR_3)_2]$,[18] and have used them as catalytic precursors.[19,20] An electrochemical study of the complexes has demonstrated a direct relationship between $E°$ for the Ru^{III}/Ru^{II} couple and their catalytic activity.[20] Modification of the nature of the charge-compensating group results in $E°$ tuning in the complex. In addition, and unlike the Cp^- ion, the charge-compensated monoanionic carborane ligands are capable of stabilizing Rh^I and Rh^{III} complexes.[21]

Here we report the preparation of Ni^{II}, Co^{II}, Co^{III}, Ru^{II} and Fe^{II} sandwich complexes of [10-SMe_2-7,8-*nido*-$C_2B_9H_{10}]^-$, along with their spectroscopic and electrochemical properties. Comparison between metallocenes and Dcb^{2-} sandwich complexes is discussed. Additionally, the energy profile and energy rotation barriers have been theoretically and experimentally calculated, and compared with data from X-ray diffraction single-crystal analyses. We also discuss conformational habits based on $\mathbf{2}^+$ and **5**.

Results and Discussion

Syntheses and NMR studies: Reaction of $NiCl_2 \cdot 6H_2O$ with a solution of K[10-SMe_2-7,8-*nido*-$C_2B_9H_{10}$] in ethanol[18] at room temperature yielded a yellow suspension, from which the paramagnetic complex *commo*-[3,3′-Ni(8-SMe_2-1,2-$C_2B_9H_{10})_2$] (**1**) was isolated as an analytically pure solid in 66% yield (Scheme 1). In contrast to *commo*-[3,3′-Ni(1,2-$C_2B_9H_{11})_2]^{2-}$, which is air sensitive and readily oxidises to a Ni^{III} complex,[4] **1** is air- and moisture-stable in solution and in the solid state. The elemental analysis for **1** is in agreement with the proposed stoichiometry. The paramagnetic nature of **1** is evidenced by the broad $^{11}B\{^1H\}$ NMR spectrum that extends from $\delta = +140$ to -120 ppm. Moreover, no evidence of B–H coupling is observed in the ^{11}B NMR spectrum. The ^1H NMR spectrum shows B–H and C–H broad resonances from $\delta = +85$ to -170 ppm. The IR spectrum of **1** shows ν(B–H) at 2518 cm^{-1}. The UV-visible spectral data of **1** in acetonitrile are given in Table 1, and consist of five absorptions at 217, 257, 351, 495 and 745 nm.

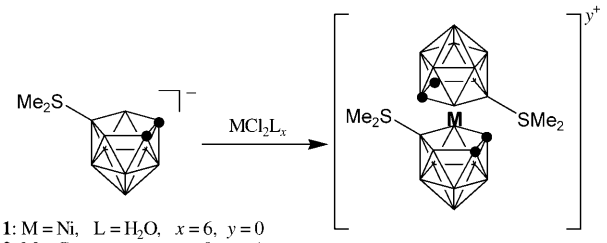

1: M = Ni, L = H_2O, $x = 6$, $y = 0$
2: M = Co, $x = 0$, $y = 1$
4: M = Ru, L = dmso, $x = 4$, $y = 0$
5: M = Fe, L = dppe, $x = 1$, $y = 0$

Scheme 1. Formation of *commo*-[3,3′-M(8-SMe_2-1,2-$C_2B_9H_{10})_2$].

Table 1. UV-visible spectral data (nm) for complexes **1**–**5** in CH_3CN.

	λ (ε)
1	217[a] (11300), 257[a] (6700), 351 (12000), 495 (85), 745 (54)
$\mathbf{2}^+$	215[a] (5900), 250[a] (6100), 300 (23700), 464 (280)
3	222 (17800), 265 (11400), 339 (9500), 442 (220)
4	198 (54000), 223 (37000), 336[a] (30), 362 (610), 481 (60)
5	221 (32200), 268[a] (8900), 383 (130), 520 (180)

[a] Shoulder.

The Co^{III} complex was similarly prepared by mixing K[10-SMe_2-7,8-*nido*-$C_2B_9H_{10}$] and anhydrous $CoCl_2$ in MeOH or EtOH yielding the orange diamagnetic complex *commo*-[3,3′-Co(8-SMe_2-1,2-$C_2B_9H_{10})_2$]Cl (**2**-Cl; Scheme 1). The [10-SMe_2-7,8-*nido*-$C_2B_9H_{10}]^-$ ligand behaves in a similar manner to [7,8-*nido*-$C_2B_9H_{11}]^{2-}$[4,5] in that it stabilizes a Co^{III} complex. Formation of $\mathbf{2}^+$ was associated with the precipitation of a black residue of Co^0, suggesting the formation of an initial Co^{II} complex, which disproportionates to Co^{III} and cobalt metal.[4] Complex **2**-Cl was not isolated, but was characterised in solution by ^1H and ^{11}B NMR spectroscopy. The ^1H resonances at $\delta = 4.96$ ppm, assigned to the $C_{cluster}$–H protons, and at $\delta = 2.84$ ppm due to the SMe_2 protons are worth noting. The $^{11}B\{^1H\}$ NMR spectrum displays a ratio pattern 2:2:8:4:2 in the range $\delta = +10$ to -20 ppm (Table 2), similar to that exhibited for the parent *commo*-[3,3′-Co(1,2-$C_2B_9H_{11})_2]^-$ ion.[22] The lower field resonance is not split in the ^{11}B NMR spectrum, and is assigned to the substituted B8 atom. From low-to-high field, the resonances were assigned by means of COSY measurements to B(8,8′), B(10,10′), B(4,4′,7,7′,9,9′,12,12′), B(5,5′,11,11′) and B(6,6′) (Table 2). As expected, the presence of the positively charged SMe_2 group bonded to the B8 atom leads to a shift in all resonances, except that at $\delta = -5.4$ ppm, of approximately 3 ppm to lower field with respect to the corresponding ones in *commo*-[3,3′-Co(1,2-$C_2B_9H_{11})_2$].[23] The UV-visible spectral data for **2**-Cl in acetonitrile are displayed in Table 1, and consist of four absorptions at 215, 250, 300 and 464 nm. To our knowledge, the only cationic cobaltacarborane sandwich reported in the literature is the highly sensitive complex *commo*-[3,3′-Co{4-(4″-$(C_5H_4N)CO_2CH_3$)-1,2-$C_2B_9H_{10}\}_2]^+$, synthesised by Hawthorne and co-workers in low yield.[15d]

Table 2. $^{11}B\{^1H\}$ NMR chemical shifts (ppm) for d^6 complexes.

Boron atom	[3,3-Co(1,2-$C_2B_9H_{11})_2$]	$\mathbf{2}^+$	**4**	**5**
B8,B8′	6.5	9.7	2.0	0.8
B10,B10′	1.4	4.3	−5.4	−9.6
B4,B7,B4′,B7′	−6.0	−5.4	−9.5	−12.0
B9,B12,B9′,B12′	−6.0	−5.4	−15.0	−14.9
B5,B11,B5′,B11′	−17.2	−13.8	−22.7	−23.1
B6,B6′	−22.7	−19.8	−24.7	−26.2

With the 2^+ available, we thought that we might be able to produce the first salt fully based on cobaltabis(dicarbollide) salt. With this in mind, complex **2**-Cl was mixed with *commo*-[3,3′-Co(1,2-$C_2B_9H_{11})_2$]$^-$ to give **2**-[3,3′-Co(1,2-$C_2B_9H_{11})_2$] in 65% yield. The salt **2**-[3,3′-Co(1,2-$C_2B_9H_{11})_2$] was fully characterised by elemental analysis, IR and NMR spectroscopy. The $^{11}B\{^1H\}$ NMR spectrum consists of a 2:2:2:2:16:4:4:2:2 pattern from low-to-high field that is the sum of the spectra of the two individual ions; this indicates that no interaction between these two C_{2v} symmetry moieties exists in solution at room temperature. The $^1H\{^{11}B\}$ NMR spectrum at room temperature can be interpreted in a similar way. The IR spectrum shows an intense broad band centred at 2535 cm^{-1} assigned to the B–H stretching vibrations.

The Co^{II} sandwich complex *commo*-[3,3′-Co(8-SMe_2-1,2-$C_2B_9H_{10})_2$] (**3**), the analogue to **1**, was produced in a 92% yield by reduction of **2**-Cl with metallic Zn in MeOH/H_2O. Evidence for the production of **3** was given by the cyclic voltammetry (CV) of **1** (vide infra), which shows that the redox potential is significantly more positive than in the parent analogue *commo*-[3,3-Ni(1,2-$C_2B_9H_{11})_2$]$^{2-}$, with $\Delta E°\cong 1$ V. This indicates that the reduced form of the redox couple is more stable in **1** than in the parent analogue. We would expect the same to be applicable to 2^+, thus generating a stable complex **3**. The paramagnetic nature of **3**, a d^7 complex, is evidenced by the ^{11}B NMR spectrum, which shows resonances in a wide range ($\delta = +62.8$ to -34.4 ppm) compared to the diamagnetic 2^+ ($\delta = +9.6$ to -22.2 ppm). In contrast to **1**, however, some of the B–H couplings for **3** could be observed in the ^{11}B NMR spectrum. The ^1H NMR spectrum is also widened, extending from $\delta = +26$ to -60 ppm, and is similar to the spectrum for *commo*-[3,3′-Co(1,2-$C_2B_9H_{11})_2$]$^{2-}$.[10] The electronic spectral data registered for complex **3** in acetonitrile are presented in Table 1. Four absorptions are observed at 222, 265, 339, and 442 nm in a similar range to those observed for its precursor 2^+.

The reaction of [$RuCl_2$(dmso)$_4$] with K[10-SMe_2-7,8-*nido*-$C_2B_9H_{10}$] in EtOH under reflux leads to the d^6 complex *commo*-[3,3′-Ru(8-SMe_2-1,2-$C_2B_9H_{10})_2$] (**4**; Scheme 1). The $^{11}B\{^1H\}$ NMR spectrum exhibits six resonances in the region $\delta = +2.0$ to -24.7 ppm, with area ratios 2:2:4:4:4:2. The resonance at lower field ($\delta = 2.0$ ppm), not split in the ^{11}B NMR spectrum, is assigned to the Me_2S–B8 moiety. Assignments were made with a two-dimensional (2D) $^{11}B\{^1H\}$–$^{11}B\{^1H\}$ COSY experiment and correspond to B(8,8′), B(10,10′), B(4,4′,7,7′), B(9,9′,12,12′), B(5,5′,11,11′) and B(6,6′), respectively (Table 2). The $^1H\{^{11}B\}$ NMR resonances for the SMe_2 and $C_{cluster}$–H protons are dependent on the metal's nature, and for **4** are observed at 2.47 and 3.59 ppm, respectively. The ν(B–H) absorption in the IR spectrum is found at 2559 cm^{-1}. The UV-visible spectral data for complex **4** are given in Table 1; the absorptions registered in acetonitrile are 198, 223, 336, 362, and 481 nm. In this spectrum, the two bands at 198 and 362 nm were not observed previously in complexes **1**–**3**.

Even though complex *commo*-[3,3′-Fe(8-SMe_2-1,2-$C_2B_9H_{10})_2$] (**5**) had been previously prepared from $FeCl_2$·4H_2O by Plešek and co-workers,[24] we report an improved synthesis by using [$FeCl_2$(dppe)] as a source of iron (Scheme 1). Reaction of K[10-SMe_2-7,8-*nido*-$C_2B_9H_{10}$] in THF with [$FeCl_2$(dppe)] in a 2:1 ratio leads to the formation of **5** in 63% yield, higher than the 47% reported yield.[24] Complex **5** exhibits a $^{11}B\{^1H\}$ NMR pattern 2:2:4:4:4:2 in a similar range to complex **4**, and the assignment of resonances is also the same (Table 2). In the $^1H\{^{11}B\}$ NMR spectrum the $C_{cluster}$–H proton resonances that appear at $\delta = 3.52$ and 2.50 ppm are assigned to the SMe_2 protons. The UV-visible spectrum for **4** in acetonitrile shows four absorptions at 221, 268, 383, and 520 nm (Table 1).

Computational studies and crystal structures

Theoretical studies: The room-temperature ^{11}B NMR patterns of complexes **1**–**5** may be compatible with rotamers that have either C_{2h} or C_{2v} symmetry. The main difference between these two symmetries lies in the disposition of the cluster carbon atoms. If they are in an averaged *cisoid* disposition the molecule is C_{2v}, but if they are in a *transoid* disposition the molecule is C_{2h}. The calculation of the rotational preferences of **1**–**5** were carried out by using the semiempirical ZINDO/1 computational method. The energy rotation barriers and the relative stability of the most stable rotamers can be determined from the energy profiles. Calculations were carried out for idealised models of complexes **1**–**5**, in which the SMe_2 group was substituted by SH_2. Starting from the eclipsed conformation (0°), one moiety was rotated with regard to the second at 1° intervals. The position of the SH_2 group was allowed to relax by means of molecular mechanics geometry optimisation before calculating the energy in each conformation. We expect three possible rotamer energy minima on inspection of the idealised rotamers, which are indicated as **A**, **B** and **C** in Figure 1. Rotamer **A**,

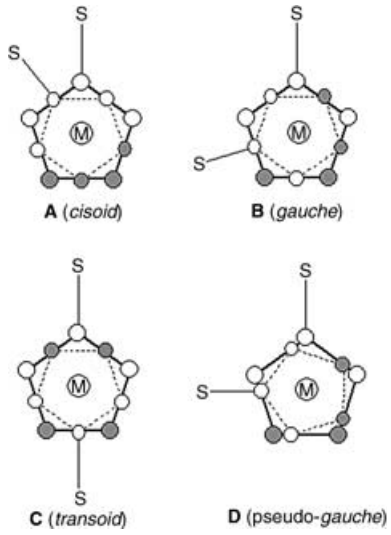

Figure 1. Mutual configuration of the zwitterionic ligands in metal complexes **1**–**5**.

which corresponds to a *cisoid* conformation, is the one with the highest steric hindrance and the one that may be subjected to the highest coulombic repulsion. All these forces may be compensated by the more electronegative atoms being in close proximity. In rotamer **B**, the clusters are mutually rotated 108°, adopting a *gauche* conformation, and would correspond to a balanced situation between steric and electronic requirements. Finally, rotamer **C**, which corresponds to a *transoid* conformation (180°), would have the minimum steric hindrance, although comparable to **B**, but would not be so favourable electronically due to the *trans* disposition of the most electronegative elements. Based on this simple model, configuration **B** would be the most stable, and the stability of **A** or **C** would provide information on the relative importance of steric hindrance versus electronic effects in these metallacarboranes.

The analysis of the calculated energy profiles for complex **1** (Figure 2), agrees with the discussion above and five different relative minima were found. As expected, the global

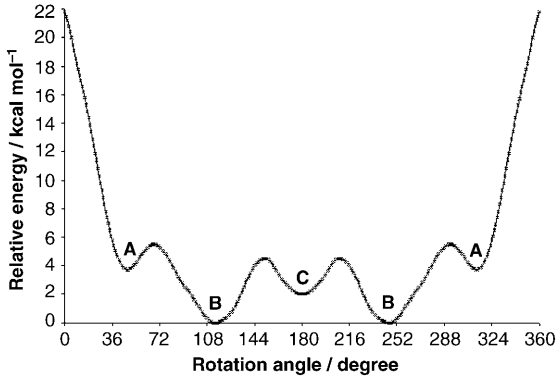

Figure 2. Calculated energy profile for compound **1** by the ZINDO/1 method.

minimum corresponds to the *gauche* configuration represented by rotamer **B** (116° and 244°). The other three relative minima are observed at 49° and 311°, rotation angles that correspond to rotamer **A**, and at 180°, corresponding to rotamer **C**. Rotamer **A** is comparable in energy to rotamer **C** and is destabilised with regard to the *gauche* conformation. Calculations yield a theoretical rotational barrier between **B** and **C** of 4.5 kcal mol^{-1} (Table 3). This is low enough to account for the symmetric appearance of the ^{11}B NMR resonances that would correspond to an averaged C_{2h} symmetry.

Table 3. Energy barriers (kcal mol^{-1}) calculated by theoretical studies.

	cisoid→*gauche*	*gauche*→*transoid*
1	5.5	4.5
2$^+$	6.8	11.5
3	5.8	5.8
4	2.2	5.2
5	6.7	8.0

This model is also valid for **2**$^+$; however for this complex the electronic and steric effects are reversed. As seen in Figure 3, five relative energy minima are observed, four are

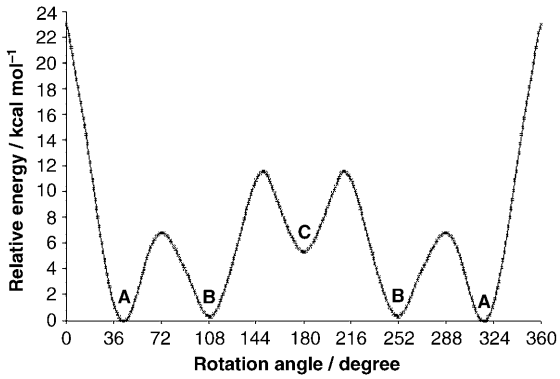

Figure 3. Calculated energy profile for complex **2**$^+$ by the ZINDO/1 method.

quasi-degenerate corresponding to rotation angles at 45° (315°) and 110° (250°), for rotamers **A** and **B**, respectively (Figure 1), whereas rotamer **C** is less stable. Two rotational barriers are detected with energy values of 6.8 and 11.5 kcal mol^{-1} (Table 3). This situation is in contrast to that for **1**, in which rotamer **B** is definitely more stable than **C** and **A**, and in which the rotational barrier is only 4.5 kcal mol^{-1}.

The analysis of the calculated energy profile for **3** is very similar to that for **1**. Five relative energy minima (at 46° (314°), 115° (245°) and 180°) are observed, two of them (**A**, **C**) being quasi-degenerate and with a rotation barrier near 5.8 kcal mol^{-1} (Table 3). The lowest energy minimum for **3** corresponds to a rotation angle near 115° (245°), which closely corresponds to the *gauche* conformation represented by the rotamer **B**.

We found a slight variation in the energy profiles for complex **4**, with regard to the other neutral **1** or **3** sandwich complexes. Seven relative energy minima corresponding to rotation angles of 48° (312°), 93° (267°), 116° (244°) and 180° are observed. However, conformations between 93° and 116° could be interpreted as belonging to a broad conformation minimum, with an almost negligible energy barrier (Figure 4). The first three minima (corresponding to **A**, **D** and **B**) are comparable in energy, although **B** is the most stable. The rotamer at 180° corresponds to **C** (Figure 1). The rotation barrier between **A** and **B** is almost negligible (2.2 kcal mol^{-1}), while the rotation barrier between **B** and **C** is also small, although slightly higher (5.2 kcal mol^{-1}) (Table 3). This is the first example in which an energy minimum at 93°, corresponding to **D** in Figure 1, has been observed for this type of sandwich complex.

Energy profiles for complex **5** are similar to those for complexes **1** and **3** (Figure 2), showing five relative energy minima. The lowest minima correspond to rotamer **B** at

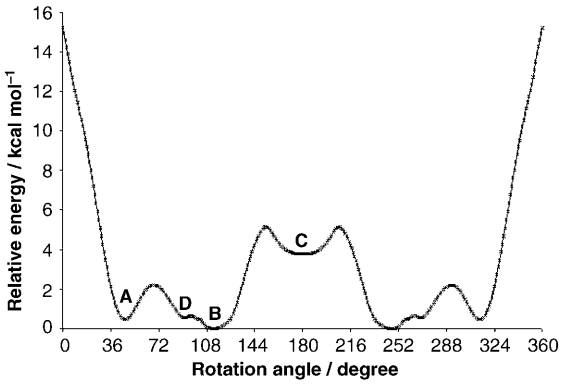

Figure 4. Calculated energy profile for compound **4** by the ZINDO/1 method.

116° and 244°. The calculated rotation barrier between **B** and **C** is 8.0 kcal mol^{-1} (Table 3).

In general, rotational energy barriers corresponding to the ring rotation in classical organometallic sandwich complexes are low (1–2 kcal mol^{-1}).[25] Incorporation of substituents on the ring increases the value; in fact, measurements carried out in mono- and 1,1′-disubstituted ferrocenes have shown energy barriers between 0.9 and 5.0 kcal mol^{-1}.[26] The calculated energy barriers for complexes **1**–**5** have been found to be between 2.2 and 11.5 kcal mol^{-1} (Table 3). These values are higher than for the metallocenes, which may be explained by the out-of-plane disposition of substituents in the C_2B_3 coordinating face and the different electronegativity of their constituents, two carbon and three boron atoms, with regard to the element's homogeneity in classical metallocenes (Figure 5).

To test the consistency of the above calculations, it has been possible to experimentally deduce the rotational barriers for complexes **2**$^+$ and **5** by dynamic NMR spectroscopy (DNMR). Coalescence of the corresponding $C_{cluster}$–H resonances is observed in the ^{1}H NMR spectra for both complexes. The $C_{cluster}$–H resonances split below the coalescence temperature (T_c) into two equal intensity resonances. Complex **2**$^+$ exhibits a T_c at 253 ± 2 K, resulting in a rotational barrier of 11.8 ± 0.2 kcal mol^{-1}. A rotational barrier of 8.3 ± 0.2 kcal mol^{-1} has been obtained for **5**, from the T_c at 183 ± 2 K. The calculated and experimental data agree very well: 11.5 versus 11.8 ± 0.2 kcal mol^{-1} for complex **2**$^+$, and 8.0 versus 8.3 ± 0.2 kcal mol^{-1} for complex **5**; these results prove the reliability of the ZINDO/1 method for this purpose.

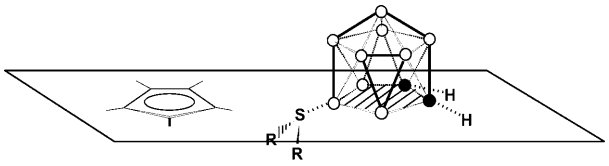

Figure 5. Projection of $[C_5H_5]^-$ and [10-SMe_2-7,8-$C_2B_9H_9$]$^-$ on the plane.

X-ray diffraction studies: Single-crystal X-ray diffraction analyses of **1**, **2**-Cl·EtOH, **3** and **4** confirmed the expected sandwich structures with the SMe_2 charge-compensating moieties connected to both B8 and B8′ atoms. The X-ray diffraction crystallographic data for these complexes is presented in Table 4. The structures are presented in Figures 6–9 and selected bond parameters are listed in Tables 5–7.

The air-stable paramagnetic d^8 complex **1** crystallised from acetonitrile, while complex **3** crystallised from a CH_2Cl_2/hexane solvent mixture under N_2 atmosphere. Both complexes were isolated as good crystals suitable for X-ray diffraction analysis (Figures 6 and 7, respectively). Complexes **1** and **3** are isostructural assuming twofold symmetry with the metal atoms lying at the symmetry axis. In complex **1**, the Ni–C and Ni–B coordination bonds are longer than the corresponding bonds in **3**, therefore the M–C_2B_3 distance in **1** (1.6709(19) Å) is longer than in **3** (1.5708(9) Å) (Table 5). The coordinating C_2B_3 belt in **3** is slightly opened (0.065 Å) relative to that of **1**. Most of the remaining bond parameters in **1** and **3** are the same within experimental error, or differ only slightly. Mutual ring rotation angles are very similar with values −112.2° and −112.8° for complexes **1** and **3**, respectively. These are in good agreement with the calculated value of 115° and confirm the *gauche* conformation (Figure 1, **B**). The structure of d^8 complex **1** is different to other d^8/d^9 metallacarboranes (M = Cu^{II}, Cu^{III}, Au^{III}, Pd^{II}, Au^{II}), which possess a distorted π-allyl structure.[27] The same is assumed for the paramagnetic *commo*-[3,3′-Ni(1,2-

Table 4. Crystallographic data and structural refinement details for compounds **1**, **2**-Cl·EtOH, **3**, and **4**.

	1	**2**-Cl·EtOH	**3**	**4**
formula	$C_8H_{32}B_{18}NiS_2$	$C_{10}H_{38}B_{18}CoClOS_2$	$C_8H_{32}B_{18}CoS_2$	$C_8H_{32}B_{18}RuS_2$
M_r	445.75	527.48	445.97	488.11
crystal system	orthorhombic	monoclinic	orthorhombic	orthorhombic
space group	$P2_12_12$ (no. 18)	$P2_1/n$ (no. 14)	$P2_12_12$ (no. 18)	$Pca2_1$ (no. 29)
a [Å]	10.937(4)	10.8062(2)	10.6787(2)	28.3728(3)
b [Å]	13.207(3)	17.9282(4)	13.1730(3)	13.7834(2)
c [Å]	8.024(2)	14.1982(4)	8.04210(10)	11.5771(2)
β [°]	90	93.8396(10)	90	90
V [Å^3]	1159.0(6)	2744.52(11)	1131.29(4)	4527.50(11)
Z	2	4	2	8
T [°C]	20	−100	−100	−100
λ [Å]	0.71073	0.71073	0.71073	0.71073
ρ [g cm^{-3}]	1.277	1.277	1.309	1.432
μ [cm^{-1}]	10.12	8.81	9.38	8.72
goodness-of-fit	1.064	1.027	1.072	1.027
$R1$[a] [$I > 2\sigma(I)$]	0.0402	0.0444	0.0292	0.0278
$wR2$[b] [$I > 2\sigma(I)$]	0.0974	0.0947	0.0672	0.0669
Flack's parameter	−0.01(3)	–	0.023(17)	0.29(3)

[a] $R1 = \Sigma ||F_o| - |F_c|| / \Sigma |F_o|$. [b] $wR2 = \{\Sigma[w(F_o^2 - F_c^2)^2] / \Sigma[w(F_o^2)^2]\}^{1/2}$.

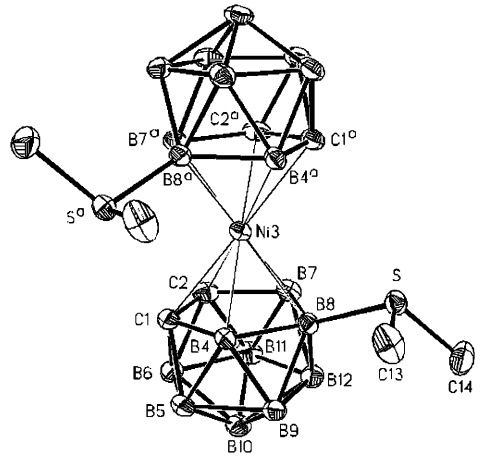

Figure 6. Drawing of compound **1** with 30% thermal displacement ellipsoids. Superscripted a refers to equivalent position $-x$, $-y$, z.

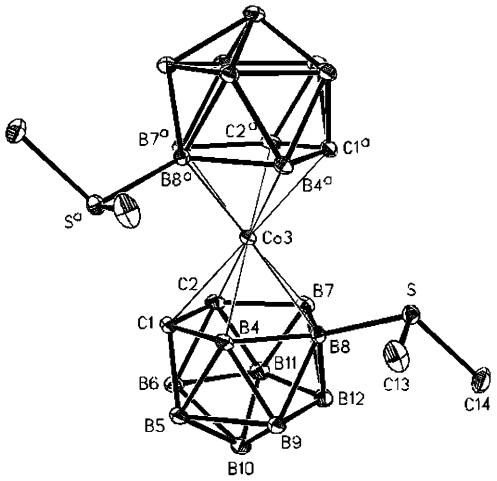

Figure 7. Drawing of **3** with 30% thermal displacement ellipsoids. Superscripted a refers to equivalent position $-x$, $-y$, z.

Table 5. Selected bond lengths (Å), angles (°) and torsion angles (°) for **1** and **3**.[a]

	1	**3**
M–C1	2.234(4)	2.1698(18)
M–C2	2.228(4)	2.092(2)
M–B8	2.194(5)	2.166(2)
S–B8	1.902(4)	1.908(2)
S–C13	1.785(4)	1.796(2)
S–C14	1.791(5)	1.795(2)
C1–C2	1.587(6)	1.592(3)
C1[a]-M-C1	176.1(2)	178.63(12)
C2[a]-M-C2	102.3(2)	101.89(11)
B8-M-B8[a]	141.5(2)	137.57(12)
S-B8-M	108.9(2)	112.20(12)
C13-S-B8-B4	25.8(4)	29.1(2)
C14-S-B8-B7	−79.9(4)	−78.1(2)
B8-c-c[a]-B8[a]	−112.2	−112.8

[a] Equivalent position $-x$, $-y$, z; c refers to centre of pentagon C1,C2,B4,B7,B8.

$C_2B_9H_{11})_2]^{2-}$ ion, the structure of which was indirectly determined, showing a "slipped" *transoid* disposition.[8b] Therefore, **1** exhibits the first crystal structure of a Ni^{II} complex sandwiched by two dicarbollide ligands; in addition the ligands adopt a *gauche* conformation. This conformation complements others already found in bis(dicarbollide)–nickel sandwich complexes. Previously the *cisoid commo*-[3,3′-Ni(1,2-$C_2B_9H_{10})_2$],[7] *transoid commo*-[3,3′-Ni(1,2-$C_2B_9H_{10})_2]^-$,[6c] or "slipped" *transoid commo*-[3,3′-Ni(1,2-$C_2B_9H_{10})_2]^{2-}$,[8b] were reported. However, complex **3** represents one of the few examples of structurally characterised Co^{II} sandwiches; until now only the d^7 Co^{II} complex [Cs_2-$(dme)_4$][Co(1,2-$C_2B_9H_{11})_2$], which has *transoid* geometry, has been studied by X-ray analysis.[10]

The diamagnetic d^6 Co^{III} complex **2**-Cl·EtOH crystallised from an EtOH/H_2O solvent mixture as orange crystals suitable for X-ray diffraction analysis (Figure 8). The structure of

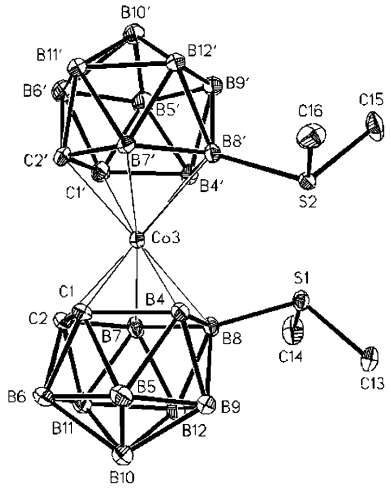

Figure 8. Drawing of complex $\mathbf{2}^+$ with 30% thermal displacement ellipsoids.

2-Cl·EtOH consists of $\mathbf{2}^+$, chloride ions and ethanol molecules, which fill the empty space in the lattice forming O–H···Cl hydrogen bonds (the O···Cl distance is 3.085(3) Å). Complex $\mathbf{2}^+$ is the first crystallographically characterised cationic cobaltacarborane, which incorporates two dicarbollide ligands. If the Co^{III} complex $\mathbf{2}^+$ is compared with Co^{II} complex **3**, we observe that the Co–C and Co–B linkages are significantly shorter in $\mathbf{2}^+$ and, consequently, the metal atom is closer to the coordinating C_2B_3 belts in $\mathbf{2}^+$ (1.4852(16) and 1.4823(16) Å) than in complex **3**. The C_2B_3 belt in $\mathbf{2}^+$ is slightly opened (0.064 Å) compared with that of **3** (see Table 6). The mutual cage configurations of upper and lower belts in $\mathbf{2}^+$ and **3** are quite different. The disposition of ligands in **3** is *gauche* (−112.8°), but *cisoid* (−40.9°) in $\mathbf{2}^+$ (see Figure 1, **A**). This disposition is also manifested in the intramolecular S···S distances (5.7025(10) Å for **3** and 3.0686(12) Å for $\mathbf{2}^+$). The S···S distance in complex $\mathbf{2}^+$ is 0.53 Å shorter than the sum of the van der Waals radii indi-

Table 6. Selected bond lengths (Å), angles (°) and torsion angles (°) for **2**-Cl·EtOH.[a]

Co3–C1	2.050(3)	S1–C13	1.785(3)
Co3–C2	2.053(3)	S1–C14	1.795(3)
Co3–B8	2.119(4)	S2–B8′	1.916(4)
Co3–C1′	2.050(3)	S2–C15	1.794(3)
Co3–C2′	2.049(3)	S2–C16	1.786(3)
Co3–B8′	2.118(3)	C1–C2	1.612(4)
S1–B8	1.925(3)		
C1′–C2′	1.610(5)	B8-Co3-B8′	99.63(14)
C1-Co3-C1′	132.02(12)	S1-B8-Co3	115.72(18)
C2-Co3-C2′	95.96(13)	S2-B8′-Co3	115.00(18)
C13-S1-B8-B4	70.3(3)	C16-S2-B8′-B7′	−35.6(3)
C14-S1-B8-B7	−32.3(3)	B8-c-c′-B8′	−40.9
C15-S2-B8′-B4′	68.9(3)		

[a] c refers to centre of pentagon C1,C2,B4,B7,B8; c′ refers to centre of C1′,C2′,B4′,B7′,B8′.

cating a weak intramolecular interaction between the sulphur atoms.[28] The mutual rotation angle found in the solid state for $\mathbf{2}^+$ agrees well with the results of theoretical calculations and is close to the energy minimum angle at 45°. A *cisoid* conformation was also found in the analogous unsubstituted d^6 *commo*-[3,3′-Co(1,2-$C_2B_9H_{11})_2]^-$ complex.[5b,29] It is important to note that the cationic complex *commo*-[3,3′-Co{4-(4″-$(C_5H_4N)CO_2CH_3$)-1,2-$C_2B_9H_{10}\}_2]^+$ has been previously described; however, no crystal structure was obtained due to its instability, which was attributed to the net positive charge.[15d]

The crystal structure of the d^6 complex *commo*-[3,3′-Ru(8-SMe_2-1,2-$C_2B_9H_{10})_2$] (**4**) corresponds to the first dicarbollide sandwich of Ru^{II}. In the asymmetric unit, there are two quasi-enantiomeric independent entities, **4a** and **4b** (Figure 9), although there is no inversion centre or mirror plane that relates the molecules. As can be seen from Table 7, most of the corresponding bond parameters in the two molecules are equal within experimental error, and minor but significant differences are observed in some bond and torsion angles. Values of −83.1° and 89.0° for mutual

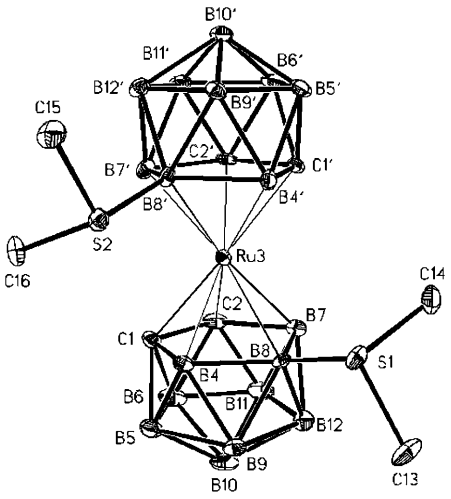

Figure 9. Drawing of **4a** with 30% thermal displacement ellipsoids.

Table 7. Selected bond lengths (Å), angles (°) and torsion angles (°) for **4**.[a]

	4a	**4b**
Ru3–C1	2.180(5)	2.181(5)
Ru3–C2	2.180(4)	2.171(5)
Ru3–B8	2.218(5)	2.234(5)
Ru3–C1′	2.170(4)	2.178(4)
Ru3–C2′	2.172(5)	2.172(4)
Ru3–B8′	2.233(5)	2.216(5)
S1–B8	1.925(5)	1.915(5)
S1–C13	1.810(5)	1.808(5)
S1–C14	1.802(5)	1.792(4)
S2–B8′	1.917(5)	1.920(5)
S2–C15	1.800(5)	1.798(5)
S2–C16	1.800(5)	1.799(5)
C1–C2	1.627(6)	1.611(6)
C1′–C2′	1.641(7)	1.630(6)
C1-Ru3-C1′	158.96(17)	96.23(19)
C2-Ru3-C2′	95.04(18)	162.92(16)
B8-Ru3-B8′	124.75(19)	126.91(19)
S1-B8-Ru3	116.2(3)	116.5(3)
S2-B8′-Ru3	116.4(3)	115.0(3)
C13-S1-B8-B4	109.4(4)	−4.0(5)
C14-S1-B8-B7	8.8(4)	−104.2(4)
C15-S2-B8′-B4′	104.5(4)	0.3(4)
C16-S2-B8′-B7′	3.7(5)	−101.6(4)
B8-c-c′-B8′	−83.1	89.0

[a] c refers to centre of C1,C2,B4,B7,B8; c′ refers to centre of C1′,C2′,B4′,B7′,B8′.

rotation angles of the carborane ligands of **4a** and **4b**, respectively, indicate a pseudo-*gauche* conformation for both complexes (see **D** in Figure 1 and Figure 4). As far as we are aware, this intermediate configuration has never been observed in a nonbridged (thus, freely rotating) bis(dicarbollyl) sandwich complex,[30] for which *cisoid*, *gauche* and *transoid* conformations have been previously defined and reported.[24,27,29] Interestingly, the experimental value for **4b** is close to the calculated value for rotamer **D**. For **4a** the mismatch with **D** is higher, but is within the **D**/**B** region in Figure 4.

The more stable rotamers obtained from the calculated energy profiles match very well with the crystal structures obtained by X-ray analysis. This suggests that only intramolecular forces are relevant to determine the most stable conformer. When two minima are in dispute, as is the case for $\mathbf{2}^+$, coulombic and ionic forces are probably responsible for the adoption of the *cisoid* conformation.

Electrochemical studies: The results shown in the former sections imply that [10-SMe_2-7,8-*nido*-$C_2B_9H_{10}]^-$ tends to produce complexes in which the metal is in a lower oxidation-state than their analogues derived from [7,8-*nido*-$C_2B_9H_{12}]^{2-}$. The redox behaviour of the metal complexes of [10-SMe_2-7,8-*nido*-$C_2B_9H_{10}]^-$ should corroborate these observations.

Cyclic voltammetry measurements were conducted on **1**, **3**, **4** and **5**, in acetonitrile by using $[NBu_4][PF_6]$ as the supporting electrolyte. The inspected range, between −2.5 and

+2.0 V with reference to the $[Cp_2Fe]^+/[Cp_2Fe]$ couple, gave rise to fully reversible diffusion-controlled processes. All CV traces have shown similar ΔE_p values as for the $[Cp_2Fe]^+/[Cp_2Fe]$ couple under the same working conditions. Hence, each process was assumed to have one-electron stoichiometry, as determined indirectly by comparison of their CV peak heights and ΔE_p values.

The data in Table 8 shows that each electrochemical process voltage for **1**, **3**, **4** and **5** is shifted by around +1 V to more positive values when compared to the equivalent process voltage in the parent bis(dicarbollide) analogues. This considerable shift accounts for the air stability of the Ni^{II} and Fe^{II} complexes, as well as the easy preparation of the Co^{II} complex. Moreover, the $E_{1/2}$ values are anodically shifted (+0.12 to +0.79 V) with regard to their metallocene analogues. Consequently it follows that the [10-SMe_2-7,8-*nido*-$C_2B_9H_{10}]^-$ ligand is more capable of stabilizing low oxidation states than the dicarbollide or cyclopentadienyl systems. A comparable phenomenon has been reported for other monoanionic heteroborane ligands, such as $[MeC_3B_7H_9]^-$ and $[CB_9H_{10}PMe]^-$.[31]

Table 8. Data obtained from cyclic studies in acetonitrile. The $[FeCp_2]^+/[FeCp_2]$ couple was taken as the zero reference.

	$E_{1/2}$ [V]			
	M^{IV}/M^{III} (IP_4)	M^{III}/M^{II} (IP_3)	M^{II}/M^{I} (IP_2)	Ref.
[3,3-Ni($C_2B_9H_{11}$)$_2$]	−0.17	−1.01	−2.52	[4,37]
[$NiCp_2$]	0.39[b]	−0.41	−2.27	[38]
[3,3-Ni(8-SMe_2-$C_2B_9H_{10}$)$_2$] (**1**)	0.87	−0.04	−1.48	this work
[3,3-Co($C_2B_9H_{11}$)$_2$]$^-$	1.16	−1.83	−2.71	[4,39]
[$CoCp_2$]	2.73[a]	−1.32[b]	−2.33[b]	[38]
[3,3-Co(8-SMe_2-$C_2B_9H_{10}$)$_2$] (**3**)		−0.77	−1.65	this work
[$RuCp_2$]		0.46[c]		[33]
[3,3-Ru(8-SMe_2-$C_2B_9H_{10}$)$_2$] (**4**)		0.62		this work
[3,3′-Fe($C_2B_9H_{11}$)$_2$]$^{2-}$		−0.84		[4,37]
[$FeCp_2$]		0		
[3,3-Fe(8-SMe_2-$C_2B_9H_{10}$)$_2$] (**5**)		0.12		this work

[a] In liquid SO_2. [b] In THF. [c] 0.1 M $[NBu_4][B(C_6F_5)_4]$ as supporting electrolyte in THF.

A complementary insight was derived from the analysis of the linear dependence of the standard potential values (E_j^o) with the metal ionisation potentials (IP_j). The equation[32] $E_j^o(V \text{ versus } Cp_2Fe) \approx a_i + 0.11\,IP_j$ is valid for sandwich complexes, thus applies for $[M(Cp)_2]$ and *commo*-[3,3′M-(1,2-$C_2B_9H_{11}$)$_2$] complexes, and expectedly for complexes derived from [10-SMe_2-7,8-*nido*-$C_2B_9H_{10}]^-$. In the equation, a_i is a constant that is characteristic of each ligand (−3.18 for $[C_5H_5]^-$ and −3.68 for [7,8-*nido*-$C_2B_9H_{11}]^{2-}$) and j= 1,2,….[4,13,33] The a_i constant is related to the electronic stabilizing effect of the π ligand, making it useful for comparison purposes. As expected, the E_j^o against IP_j plot for **1**, **3**, **4** and **5** revealed that the ligand [10-SMe_2-7,8-*nido*-$C_2B_9H_{10}]^-$ also displays a similar linear behaviour with a slope (a_i) of −2.70, hence $a_i([10\text{-}SMe_2\text{-}7,8\text{-}nido\text{-}C_2B_9H_{10}]^-) > a_i([C_5H_5]^-) > a_i([7,8\text{-}nido\text{-}C_2B_9H_{11}]^{2-})$.

These results confirm that this charge-compensated ligand is more capable of stabilising lower oxidation states in metals, such as Ni^{II}, Co^{II}, Ru^{II} and Fe^{II}, than Dcb^{2-} ligand and even Cp^- ligand. This has been demonstrated with the preparation of the above complexes.

Conclusion

The first paramagnetic Ni^{II} and Co^{II} and diamagnetic Ru^{II} and Co^{III} sandwich complexes, which contain the charge-compensated [10-SMe_2-7,8-*nido*-$C_2B_9H_{10}]^-$ ligand, have been successfully prepared by the direct reaction of the carborane anion with the appropriate metal source. The electrochemical data indicate that the incorporation of the positive SMe_2 group into the cluster causes a decrease of the electron-donating capacity of this ligand compared to the Dcb^{2-} and Cp^- ligands, which confirms the relatively easy stabilisation of low-oxidation-state metal complexes. Semiempirical calculations have revealed that all these sandwich complexes are compatible with several rotamers in solution, with low rotational barriers that do not hinder free relative movement of the two ligands at room temperature. Energy rotation barriers have been determined experimentally for two complexes and are in agreement with the calculations. In addition, X-ray diffraction studies for complexes **1**–**4** are coincident with ZINDO/1 calculations concerning the most stable conformer: only one rotamer is found in the solid state for **1**–**3** and two for the Ru^{II} complex **4**. All neutral complexes have revealed the unusual *gauche* or pseudo-*gauche* conformation in the solid state, probably due to steric and electronic factors. In contrast, the cationic complex $\mathbf{2}^+$ shows a *cisoid* conformation despite the presence of the two sulfonium groups; this seems to arise from interactions between both SMe_2 groups.

Experimental Section

General considerations: We performed elemental analyses using a Carlo Erba EA1108 microanalyser. IR spectra were recorded with KBr pellets on a Shimadzu FTIR-8300 spectrophotometer. UV-visible spectroscopy was carried out with a Cary 5E spectrophotometer using 0.1 cm cuvettes. The concentration of the complexes was 1×10^{-3} mol L^{-1}. ^1H and $^1H\{^{11}B\}$ NMR (300.13 MHz), $^{13}C\{^1H\}$ NMR (75.47 MHz), ^{11}B and $^{11}B\{^1H\}$ NMR (96.29 MHz) spectra were recorded at room temperature on a Bruker ARX 300 instrument equipped with the appropriate decoupling accessories. All NMR measurements were performed in $[D_6]$acetone at 22 °C. Chemical shift data for ^1H, $^1H\{^{11}B\}$ and $^{13}C\{^1H\}$ NMR spectra are referenced to $SiMe_4$, those for $^{11}B\{^1H\}$ and ^{11}B NMR spectra are referenced to external $BF_3{\cdot}OEt_2$. Chemical shifts are reported in ppm, followed by a description of the multiplet (for example, d = doublet), its relative intensity, and observed coupling-constants (in Hz).

Unless otherwise noted, all manipulations were carried out under a dinitrogen atmosphere by using standard vacuum-line techniques. Solvents were purified by distillation from appropriate drying agents before use. Deuterated solvents for NMR (Fluorochem) were freeze-pump-thawed three times under N_2 and were transferred to the NMR tube using stan-

dard vacuum-line techniques. The carborane 10-SMe_2-7,8-*nido*-$C_2B_9H_{10}$ was prepared following the literature procedure[34] and $[RuCl_2(dmso)_4]$ was prepared according to the literature.[35] All other chemicals were purchased from Fluka or Aldrich, and were used as-received.

Synthesis of *commo*-[3,3′-Ni(8-SMe_2-1,2-$C_2B_9H_{10}$)$_2$] (1): A solution of $NiCl_2{\cdot}6H_2O$ (162 mg, 0.682 mmol) in EtOH (2 mL) was added dropwise to a Schlenk flask charged with a solution of 10-SMe_2-7,8-*nido*-$C_2B_9H_{11}$ (26.6 mg, 0.137 mmol) and K[*t*BuO] (24 mg, 0.204 mmol) in EtOH (4 mL). The yellow suspension was stirred for 5 min, concentrated in vacuo to 1 mL, and cooled to 0 °C. The resultant yellow solid was isolated by filtration, washed with cold EtOH (2×2 mL), and dried in vacuo to afford 20 mg (66 %) of complex **1**. Yellow crystals suitable for an X-ray diffraction study were grown by slow evaporation of a solution of **1** in acetonitrile at room temperature. $^1H\{^{11}B\}$ NMR: $\delta = 84.3$, 24.4, 6.9, −134.4, −156.7, −170.0 ppm; $^{11}B\{^1H\}$ NMR: $\delta = 139.2$, 72.6, 71.5, −26.2, −116.3 ppm; IR: $\tilde{\nu} = 2560$, 2537, 2528 cm^{-1} (B–H); elemental analysis calcd (%) for $C_8H_{32}B_{18}NiS_2$: C 21.6, H 7.2, S 14.4; found: C 21.7, H 7.3, S 13.6.

Synthesis of *commo*-[3,3′-Co(8-SMe_2-1,2-$C_2B_9H_{10}$)$_2$]Cl ([2]-Cl): A solution of $CoCl_2$ (57.0 mg, 0.439 mmol) in MeOH (4 mL) was added dropwise to a solution of 10-SMe_2-7,8-*nido*-$C_2B_9H_{11}$ (51.4 mg, 0.265 mmol) and K[*t*BuO] (54.4 mg, 0.460 mmol) in MeOH (6 mL). Immediately, a dark yellow solution was observed, from which a yellow solid precipitated. The precipitate's colour changed to green on addition of water (6.5 mL). The mixture was filtered and washed with MeOH/H_2O (60:40, 15 mL). The remaining greenish solid was treated with a mixture of a NaCl solution (5 mL, 3 M), HCl (6 mL, 2.4 M), and ethyl acetate (5 mL) to afford a yellow solid and a red solution. The solid was completely dissolved in ethyl acetate (10 mL) and was transferred to a separating funnel together with the red solution. After shaking and allowing the layers to separate, the aqueous red layer was discarded and the organic phase was smoothly heated under moderately reduced pressure for 5 min, causing the precipitation of an orange solid. This was collected and dissolved in MeOH/H_2O (60:40, 10 mL). Orange crystals of **2**-Cl suitable for an X-ray diffraction study were grown by slow evaporation of this solution at room temperature. $^1H\{^{11}B\}$ NMR: $\delta = 4.9$ (br s, 4H; C_c-*H*), 2.84 ppm (s, 12H; S-CH_3); $^{11}B\{^1H\}$ NMR: $\delta = 9.7$ (2B), 4.3 (2B), −5.4 (8B), −13.8 (4B), −19.8 ppm (2B); ^{11}B NMR: $\delta = 9.7$ (2B), 4.3 (d, *J*(H,B) = 135 Hz; 2B), −5.4 (8B), −13.8 (d, *J*(H,B) = 157 Hz; 4B), −19.8 ppm (2B).

Synthesis of *commo*-[3,3′-Co(8-SMe_2-1,2-$C_2B_9H_{10}$)$_2$][3,3′-Co(1,2-$C_2B_9H_{11}$)$_2$], (2-[3,3′-Co(1,2-$C_2B_9H_{11}$)$_2$]): A solution of [Cs{3,3′-Co(1,2-$C_2B_9H_{11}$)$_2$}] (90.0 mg, 0.197 mmol) in MeOH/H_2O (60:40, 10 mL) was added to the solution containing complex **2**-Cl in MeOH/H_2O (60:40, 10 mL), prepared as described above starting from 10-SMe_2-7,8-*nido*-$C_2B_9H_{11}$ (51.4 mg, 0.265 mmol). The resultant orange solid was filtered and washed with MeOH/H_2O (60:40, 10 mL) to afford 66 mg of **2**-[3,3′-Co(1,2-$C_2B_9H_{11}$)$_2$] (yield 65 %). $^1H\{^{11}B\}$ NMR: $\delta = 4.96$ (br s, 4H; C_c-*H*), 3.96 (br s, 4H; C_c-*H*), 2.84 ppm (s, 12H; S-CH_3); $^{11}B\{^{11}H\}$ NMR: $\delta = 9.6$ (2B), 7.1 (2B), 4.3 (2B), 1.9 (2B), −5.4 (16B), −13.7 (4B), −16.7 (4B), −19.7 (2B), −22.2 ppm (2B); ^{11}B NMR: $\delta = 9.6$ (s, 2B), 7.1 (d, *J*(H,B) = 141 Hz; 2B), 4.3 (d, *J*(H,B) = 142 Hz; 2B), 1.9 (d, *J*(H,B) = 136 Hz; 2B), −5.4 (16B), −13.7 (d, *J*(H,B) = 167 Hz; 4B), −16.7 (d, *J*(H,B) = 157 Hz; 4B), −19.7 (2B), −22.2 ppm (d, *J*(H,B) = 173 Hz; 2B); IR: $\tilde{\nu} = 2589$, 2557, 2535, 2501 cm^{-1} (B–H); elemental analysis calcd (%) for $C_{12}H_{54}B_{36}Co_2S_2$: C 18.7, H 7.0, S 8.3; found: C 19.0, H 6.97, S 7.2.

Synthesis of *commo*-[3,3′-Co(8-SMe_2-1,2-$C_2B_9H_{10}$)$_2$] (3): The synthesis procedure was the same as for **2**-Cl, but using $CoCl_2$ (418 mg, 3.22 mmol) in MeOH (8 mL), and 10-SMe_2-7,8-*nido*-$C_2B_9H_{11}$ (125 mg, 0.644 mmol) and K[*t*BuO] (152 mg, 1.287 mmol) in MeOH (10 mL). The workup was followed up to get a solution of *commo*-[3,3′-Co(8-SMe_2-1,2-$C_2B_9H_{10}$)$_2$]Cl in MeOH/H_2O (60:40; 100 mL). Activated metallic Zn (211 mg, 3.23 mmol) was added to the solution and the mixture was stirred overnight and the colour of the solution faded. The solid was filtered, partially dissolved in CH_2Cl_2 and treated with an excess of hexane. The resulting greyish solid was collected by filtration, under N_2, to afford 86 mg of complex **3** (60 %). Crystals of complex **3** suitable for X-ray diffraction analysis were grown from a solution of **3** in CH_2Cl_2/hexane (1:1), under an N_2 atmosphere. $^1H\{^{11}B\}$ NMR: $\delta = 26.6$, 3.43, 2.87, 2.10, 7.50, 7.80, −37.55, −44.76, −59.43 ppm; $^{11}B\{^1H\}$ NMR: $\delta = 62.8$ (4B), 51.2 (2B), 11.8 (2B), −30.6 (4B), −34.4 ppm (6B); ^{11}B NMR: $\delta = 62.8$ (4B), 51.2 (2B), 11.8 (d, *J*(H,B) = 138 Hz; 2B), −30.6 (d, *J*(H,B) = 143 Hz; 4B), −34.4 ppm (d, *J*(H,B) = 129 Hz; 6B); IR: $\tilde{\nu} = 2621$, 2578, 2548, 2518 cm^{-1} (B–H); elemental analysis calcd (%) for $C_8H_{32}B_{18}CoS_2$: C 21.6, H 7.2, S 14.4; found: C 21.7, H 7.3, S 13.6.

Synthesis of *commo*-[3,3′-Ru(8-SMe_2-1,2-$C_2B_9H_{10}$)$_2$] (4): $[RuCl_2(dmso)_4]$ (60 mg, 0.129 mmol) was added to a solution of 10-SMe_2-7,8-*nido*-$C_2B_9H_{10}$ (25 mg, 0.129 mmol) and K[*t*BuO] (16 mg, 0.135 mmol) in EtOH (5 mL). The mixture was refluxed overnight to give a brown solid. The solid was filtered and dissolved in acetone. The resultant yellow solution was concentrated in volume and treated with an excess of hexane. The resulting yellow solid was collected by filtration to yield 22 mg of complex **4** (70 %). Crystals suitable for an X-ray diffraction study were grown from a solution of **4** in acetone/$CHCl_3$ 2:1. $^1H\{^{11}B\}$ NMR: $\delta = 3.59$ (br s, 4H; C_c-*H*), 2.47 ppm (s, 12H; SCH_3); $^{11}B\{^1H\}$ NMR: $\delta = 1.9$ (1B), −5.4 (1B), −9.5 (2B), −15.0 (2B), −22.7 (2B), −24.7 ppm (1B); ^{11}B NMR: $\delta = 1.9$ (s, 1B), −5.4 (d, *J*(H,B) = 141 Hz; 1B), −9.5 (d, *J*(H,B) = 145 Hz; 2B), −15.0 (d, *J*(H,B) = 135 Hz; 2B), −22.7 (d, *J*(H,B) = 159 Hz; 2B), −24.7 ppm (d, *J*(H,B) = 189 Hz; 1B); IR: $\tilde{\nu} = 2611$, 2559, 2522, 2491 cm^{-1} (B–H); elemental analysis calcd (%) for $C_8H_{32}B_{18}RuS_2$: C 19.6, H 6.6, S 13.1; found: C 19.7, H 6.7, S 13.1.

Synthesis of *commo*-[3,3′-Fe(8-SMe_2-1,2-$C_2B_9H_{10}$)$_2$] (5): $[FeCl_2(dppe)]$ (80 mg, 0.152 mmol) was added to a solution of 10-SMe_2-7,8-*nido*-$C_2B_9H_{10}$ (48.7 mg, 0.251 mmol) and BuLi (0.15 mL, 0.270 mmol) in THF (2 mL) to give a violet solution. After refluxing for 30 min, the solvent was evaporated and EtOH (5 mL) was added. The resultant violet precipitate was filtered and was washed with EtOH (5 mL). The solid was dried in vacuo to yield 35 mg of compound **5** (63 %).

Calculation details: All calculations were performed using the Hyperchem 5.0 package (Version 5.0, Hyperchem Inc.) installed on a PC-Pentium III 700 MHz personal computer. Calculations were performed on an idealised model in which the SMe_2 group was approximated by SH_2 (S–H 1.42 Å). The distances were set up as B–B = 1.78 Å, B–C = 1.70 Å, C–C = 1.60 Å and B–H = C–H = 1.12 Å. After introduction of a metal, the C_2B_3 coordinating faces were situated in a parallel and centred disposition. The metal is equidistant from the two carbon atoms and the B8 atom. The difference in ring separation between ferracarborane *commo*-[3,3′Fe(8-SMe_2-1,2-$C_2B_9H_{10}$)$_2$] (2.089 Å) and the $[Fe(Cp)_2]$ (2.064 Å) was assumed to arise exclusively from the ligand exchange. The above subtraction (0.025 Å) was added to the corresponding distances for each metallocene. From the starting position, rotations of 1° were performed (from $\alpha = 0°$ to $\alpha = 360°$). At each point, a single-point calculation was performed using the ZINDO/1 semiempirical method. Before the ZINDO/1 calculations, the sulfonium group was allowed to relax by means of molecular mechanics geometry optimisation. All energy values correspond to free enthalpy referred to the lowest energy rotamer.

Electrochemical procedure: Cyclic voltammograms were recorded on a EG & G PAR273 A potentiostat–galvanostat. Electrochemical measurements were performed in a standard double-compartment three-electrode cell. A 4 mm^2 platinum plate and a platinum wire were used as working and counter electrodes, respectively. For standard cyclic voltammetric measurements, a silver wire was utilised as a quasi-reference electrode, and potentials were calibrated against the ferrocene from which the $E°([FeCp_2]/[FeCp_2]^+) = 0.424$ V versus the SCE. All measurements were performed on a 1 mM solution of complex in acetonitrile with tetrabutylammonium hexafluorophosphate (0.2 M) as supporting electrolyte. Cyclic voltammograms were recorded with a scan-rate of 50 $mV\,s^{-1}$. $E_{1/2}$ = half potential, calculated as the average value between oxidation- and reduction-wave potentials.

X-ray crystallography: Single-crystal data collection for complex **1** was carried out on a CAD4 diffractometer at 20 °C, while data collection for **2**-Cl·EtOH, **3** and **4** was performed at −100 °C on an Enraf Nonius Kappa CCD diffractometer using graphite-monochromatised $Mo_{K\alpha}$ radiation. A total of 1555, 4832, 2490, and 5931 unique reflections were collected for **1**, **2**-Cl·EtOH, **3** and **4**, respectively.

The structures were solved by direct methods and refined on F^2 by the SHELXL97 program.[36] Non-hydrogen atoms were refined with anisotropic thermal displacement parameters, but hydrogen atoms were treated as riding atoms using the SHELX97 default parameters. Complexes **1**, **3** and **4** crystallise in non-centrosymmetric space groups and absolute configurations were determined by refinement of Flack's χ parameter.

CCDC-234459 (**1**), CCDC-234460 (**2**-Cl·EtOH), CCDC-234461 (**3**) and CCDC-234462 (**4**) contain the supplementary crystallographic data for this paper. These data can be obtained free of charge from The Cambridge Crystallographic Data Centre via www.ccdc.cam.ac.uk/data_request/cif.

Acknowledgements

This work has been supported by MCyT, MAT2004–01108 and Generalitat de Catalunya, 2001/SGR/00337. We thank the MCyT for an FPI grant from the project MAT98–0921.

[1] a) Z. Xie, *Coord. Chem. Rev.* **2002**, *231*, 23; b) R. N. Grimes in *Comprehensive Organometallic Chemistry II*, *Vol. 1* (Eds.: E. W. Abel, F. G. A. Stone, G. Wilkinson), Pergamon, Oxford, **1995**, pp. 373–430; c) R. N. Grimes, *Coord. Chem. Rev.* **2000**, *200–202*, 773; d) A. K. Saxena, N. S. Hosmane, *Chem. Rev.* **1993**, *93*, 1081; e) A. K. Saxena, J. A. Maguire, N. S. Hosmane, *Chem. Rev.* **1997**, *97*, 2421.

[2] a) *Contemporary Boron Chemistry* (Eds.: M. Davidson, A. K. Hughes, T. B. Marder, K. Wade), Royal Society of Chemistry, Cambridge (UK), **2000**. b) W. E. Siebert in *Advances in Boron Chemistry*, Royal Society of Chemistry, Cambridge (UK), **1997**. c) *Boron Chemistry at the Beginning of the 21st Century* (Ed.: Yu. N. Bubnov), Nauka, Moscow, **2003**. d) J. Casanova, *The Borane, Carborane, Carbocation Continuum*, Wiley-Interscience, New York, **1998**; e) C. E. Housecroft in *Specialist Periodical Reports in Organometallic Chemistry* (Eds.: E. W. Abel, F. G. A. Stone), Royal Society of Chemistry, London (UK) **1991**.

[3] a) M. F. Hawthorne, D. C. Young, P. A. Wegner, *J. Am. Chem. Soc.* **1965**, *87*, 1818; b) M. F. Hawthorne, T. D. Andrews, *Chem. Commun. (London)* **1965**, 443; c) W. M. Maxwell, V. R. Miller, R. N. Grimes, *Inorg. Chem.* **1976**, *15*, 1343; d) W. M. Maxwell, V. R. Miller, R. N. Grimes, *J. Am. Chem. Soc.* **1976**, *98*, 4818.

[4] M. F. Hawthorne, D. C. Young, T. D. Andrews, D. V. Howe, R. L. Pilling, A. D. Pitts, M. Reintjes, L. F. Warren, Jr., P. A. Wegner, *J. Am. Chem. Soc.* **1968**, *90*, 879.

[5] a) A. Zalkin, T. P. Hopkins, D. H. Templeton, *Inorg. Chem.* **1967**, *6*, 1911; b) L. Borodinsky, E. Sinn, R. N. Grimes, *Inorg. Chem.* **1982**, *21*, 1686.

[6] a) L. F. Warren, Jr., M. F. Hawthorne, *J. Am. Chem. Soc.* **1967**, *89*, 470; b) M. F. Hawthorne, L. F. Warren, Jr., *J. Am. Chem. Soc.* **1970**, *92*, 1157; c) F. V. Hassen, R. G. Hazell, C. Hyatt, G. D. Stucky, *Acta Chem. Scand.* **1973**, *27*, 1210; d) M. F. Hawthorne, J. I. Zink, J. M. Skelton, M. J. Bayer, C. Liu, E. Livshits, R. Baer, D. Neuhauser, *Science* **2004**, *303*, 1849.

[7] D. St. Clair, A. Zalkin, D. H. Templeton, *J. Am. Chem. Soc.* **1970**, *92*, 1173.

[8] a) R. M. Wing, *J. Am. Chem. Soc.* **1967**, *89*, 5599; b) R. M. Wing, *J. Am. Chem. Soc.* **1968**, *90*, 4828; c) L. F. Warren, Jr., M. F. Hawthorne, *J. Am. Chem. Soc.* **1968**, *90*, 4823.

[9] a) H. W. Ruhne, M. F. Hawthorne, *Inorg. Chem.* **1968**, *7*, 2279; b) D. St. Clair, A. Zalkin, D. H. Templeton, *Inorg. Chem.* **1971**, *10*, 2587.

[10] R. M Chamberlin, B. L. Scott, M. M. Melo, K. D. Abney, *Inorg. Chem.* **1997**, *36*, 809.

[11] a) H. Zhang, Y. Wang, A. K. Sexena, A. R. Oki, J. A. Maguire, N. S. Hosmane, *Organometallics* **1993**, *12*, 3933; b) N. S. Hosmane, Y. Wang, A. R. Oki, H. Zhang, J. A. Maguire, *Organometallics* **1996**, *15*, 626; c) S. Tomlinson, C. Zheng, N. S. Hosmane, J. Yang, Y. Wang, H. Zhang, T. G. Gray, T. Demissie, J. A. Maguire, F. Baumann, A. Klein, B. Sarkar, W. Kaim, W. N. Lipscomb, *Organometallics* **2005**, *24*, 2177.

[12] D. A. Brown, M. O. Fanning, N. J. Fitzpatrick, *Inorg. Chem.* **1978**, *17*, 1620.

[13] W. E. Geiger in *Metal Interactions with Boron Clusters* (Ed.: R. N. Grimes), Plenum, New York, **1982**, p. 239.

[14] R. J. Wilson, L. F. Warren, Jr., M. F. Hawthorne, *J. Am. Chem. Soc.* **1969**, *91*, 758.

[15] a) F. N. Tebbe, P. M. Garret, M. F. Hawthorne, *J. Am. Chem. Soc.* **1968**, *90*, 869; b) D. C. Young, D. V. Hove, M. F. Hawthorne, *J. Am. Chem. Soc.* **1969**, *91*, 859; c) J. Plešek, J. Zbynek, S. Hermánek, *Collect. Czech. Chem. Commun.* **1978**, *43*, 2862; d) H. C. Kang, S. S. Lee, C. B. Knobler, M. F. Hawthorne, *Inorg. Chem.* **1991**, *30*, 2024; e) J. Plešek, T. Jelínek, F. Mareš, S. Hermánek, *Collect. Czech. Chem. Commun.* **1993**, *58*, 1534; f) G. M. Rosair, A. J. Welch, A. S. Weller, S. K. Zahn, *J. Organomet. Chem.* **1997**, *536*, 299; g) S. Dunn, R. M. Garrioch, G. M. Rosair, L. Smith, A. J. Welch, *Collect. Czech. Chem. Commun.* **1999**, *64*, 1013; h) O. Tutusaus, F. Teixidor, R. Núñez, C. Viñas, R Sillanpää, R. Kivekäs, *J. Organomet. Chem.* **2002**, *657*, 247.

[16] M. F. Hawthorne, L. F. Warren, Jr., K. P. Callahan, N. F. Travers, *J. Am. Chem. Soc.* **1971**, *93*, 2407.

[17] a) Y.-K. Yan, D. M. P. Mingos, T. E. Müller, D. J. Williams, M. Kurmoo, *J. Chem. Soc. Dalton Trans.* **1994**, 1735; b) Y.-K. Yan, D. M. P. Mingos, T. E. Müller, M. Williams, J. Kurmoo, *J. Chem. Soc. Dalton Trans.* **1995**, 2509; c) Y.-K. Yan, D. M. P. Mingos, D. J. Williams, *J. Organomet. Chem.* **1995**, *498*, 267.

[18] O. Tutusaus, R. Núñez, F. Teixidor, C. Viñas, I. Mata, E. Molins, *Inorg. Chem.* **2004**, *43*, 6067.

[19] a) O. Tutusaus, S. Delfosse, A. Demonceau, A. F. Noels, R. Núñez, C. Viñas, F. Teixidor, *Tetrahedron Lett.* **2002**, *43*, 983; b) O. Tutusaus, S. Delfosse, F. Simal, A. Demonceau, A. F. Noels, R. Núñez, C. Viñas, F. Teixidor, *Inorg. Chem. Commun.* **2002**, *5*, 941.

[20] O. Tutusaus, C. Viñas, R. Núñez, F. Teixidor, A. Demonceau, S. Delfosse, A. F. Noels, I. Mata and E. Molins, *J. Am. Chem. Soc.* **2003**, *125*, 11830.

[21] R. Núñez, O. Tutusaus, F. Teixidor, C. Viñas, R. Kivekäs, R. Sillanpää, *Organometallics* **2004**, *23*, 2237.

[22] Z. Janoušek, J. Plešek, S. Hermánek, K. Base, L. J. Todd, W. F. Wright, *Collect. Czech. Chem. Commun.* **1981**, *46*, 2818.

[23] a) S. Hermánek, V. Gregor, B. Štibr, J. Plešek, Z. Janoušek, V. A. Antonovich, *Collect. Czech. Chem. Commun.* **1976**, *41*, 1492; b) S. Hermánek, J. Plešek, B. Štibr, *J. Chem. Soc. Chem. Commun.* **1977**, 561; c) F. Teixidor, C. Viñas, R. W. Rudolph, *Inorg. Chem.* **1986**, *25*, 3339.

[24] J. Plešek, B. Štibr, P. A. Cooke, J. D. Kennedy, T. D. McGrath, M. Thornton-Pett, *Acta Crystallogr. Sect. C* **1998**, *54*, 36.

[25] a) A. Haaland, J. E. Nilsson, *Chem. Commun. (London)* **1968**, 88; b) C. H. Holm, J. A. Ibers, *J. Chem. Phys.* **1959**, *30*, 885.

[26] L. N. Mulay, A. Attalla, *J. Am. Chem. Soc.* **1963**, *85*, 702.

[27] I. B. Sivaev, V. I. Bregadze, *J. Organomet. Chem.* **2000**, *614–615*, 27, and references therein.

[28] A. Bondi, *J. Phys. Chem.* **1964**, *68*, 441.

[29] I. B. Sivaev, V. I. Bregadze, *Collect. Czech. Chem. Commun.* **1999**, *64*, 783, and references therein.

[30] For examples of bridge sandwich complexes see A. Varadarajan, S. E. Johnson, F. A. Gomez, S. Chakrabarti, C. B. Knobler, M. F. Hawthorne, *J. Am. Chem. Soc.* **1992**, *114*, 9003, and references therein.

[31] B. V. Barnum, P. J. Carroll, L. G. Sneddon, *Organometallics* **1996**, *15*, 645.

[32] V. V. Strelets, S. V. Kukharenko, *Nouv. J. Chim.* **1985**, *8*, 785.

[33] B. R. Ramachandran, S. M. Trupia, W. E. Geiger, P. J. Carrol, L. G. Sneddon, *Organometallics* **2002**, *21*, 5078.

[34] J. Plešek, T. Jelínek, F. Mareš, S. Hermánek, *Collect. Czech. Chem. Commun.* **1993**, *58*, 1534.

[35] I. P. Evans, A. Spencer, G. Wilkinson, *J. Chem. Soc. Dalton Trans.* **1973**, 204.

[36] G. M. Sheldrick, SHELX97. University of Göttingen (Germany), **1997**.
[37] W. E. Geiger, D. E. Smith, *J. Electroanal. Chem. Interfacial Electrochem.* **1974**, *50*, 31.
[38] A. J. Bard, E. Garcia, S. Kukharenko, V. V. Strelets, *Inorg. Chem.* **1993**, *32*, 3528.
[39] I. Rojo, F. Teixidor, C. Viñas, R. Kivekäs, R. Sillanpää, *Chem. Eur. J.* **2003**, *9*, 4311.

Received: March 14, 2005
Published online: July 20, 2005

